Acta Astronautica 96 (2014) 128–137

Contents lists available at ScienceDirect

Acta Astronautica

journal homepage: www.elsevier.com/locate/actaastro

Input shaped large thrust maneuver with a tethered debris object

Lee Jasper [a,*], Hanspeter Schaub [b]

[a] Aerospace Engineering Sciences Department, 431 UCB Colorado Center for Astrodynamics Research, University of Colorado, Boulder, CO 80309-0431, USA

[b] Aerospace Engineering Sciences Department, ECNT 321, 431 UCB Colorado Center for Astrodynamics Research, University of Colorado, Boulder, CO 80309-0431, USA

ARTICLE INFO

Article history:
Received 19 June 2013
Received in revised form
16 October 2013
Accepted 6 November 2013
Available online 14 November 2013

Keywords:
Space debris
Active debris removal
Tether
Input shaping

ABSTRACT

In order to reduce the debris population in LEO, remediation is necessary. An active debris removal method is explored that utilizes fuel reserves on a recently launched upper stage to rendezvous with, and tether to, debris. The system's tethered dynamics are explored using a discretized tether model attached to six degree of freedom end bodies. The thrust output is shaped to remove the spectral energy at the natural frequencies of the tether, significantly reducing the post-burn relative motion between the vehicles. The sensitivity of the input shaping performance due to imperfect knowledge of the debris mass demonstrates that a double notch spanning multiple frequencies around the first mode is necessary to be robust to unknown debris mass. On-orbit simulations show that input shaping helps the tethered system achieve smooth oscillations about a gravity gradient alignment, reducing collision likelihood.

1. Introduction

Space debris is becoming a major concern for orbital assets. While there are about 22,000 objects currently tracked, there are many thousands of dangerous debris objects in orbit [1]. In recent years, the creation of debris is on the rise, including two major catastrophic events: the Fengyun 1C anti-satellite test (ASAT) [2] that created over 3300 objects [3] and the Cosmos–Iridium collision [4] that created over 1700 objects [5].

Because of these events and the continued heavy use of low Earth orbit (LEO), the debris cascade effect predicted by Kessler and Cour-Palais [6] is occurring [7]. Mitigation methods have been shown to be important, but offer only partial solutions to reduce the future debris environment. Active Debris Removal (ADR) of five or more large objects per year is shown to be an effective way to reduce the debris population [8]. Some proposed methods [9–14] utilize harpoons, mechanical grapples, or nets to grab the debris object. While the study of the debris capture system is beyond the scope of this paper, all of these methods are likely to use tethers to connect the debris to the ADR craft to avoid close proximity operations between the tug and a tumbling object. While tethers have been studied for years [15] and actually flown on several missions [16], their use in a high force, high thrust environment has been unexplored.

To deorbit debris, the tethers must operate in short-term high stress environments during the large thrust maneuvers ($\sim$2000 N). This paper models the tether dynamics using a series of spring–mass components to discretize the tether into multiple, small masses able to capture higher order modes of the tether (similar models used in [17,18]). The ends of the tether have two, six degree of freedom large rigid bodies: one is the ADR craft and the other is the debris. The ADR craft provides thrust that, transferred through the tether, changes the periapsis of the debris object and reduces both objects' orbital

* Corresponding author.
E-mail addresses: lee.jasper@colorado.edu (L. Jasper), hanspeter.Schaub@Colorado.edu (H. Schaub).

0094-5765/$ - see front matter © 2013 IAA. Published by Elsevier Ltd. All rights reserved.
http://dx.doi.org/10.1016/j.actaastro.2013.11.005

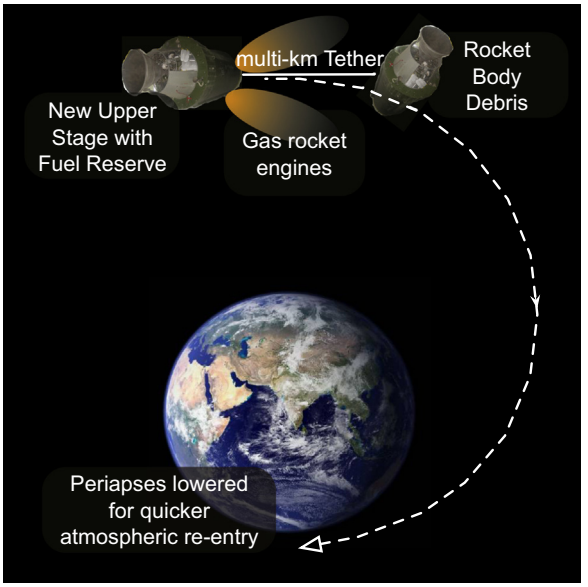

Fig. 1. Tethered tug–debris concept.

lifetimes. Ideally, the ADR craft is a rocket body with remaining fuel reserves that has recently put its payload into orbit. The remaining fuel is used to rendezvous with, and deorbit, the debris. The concept is shown in Fig. 1. Depending upon initial starting altitude and amount of fuel available to the ADR craft, the debris–tug system could be deorbited within a single orbit revolution. The tethered tug–debris architecture therefore provides a cost-effective ADR system because it deorbits two pieces of potential debris each mission.

The challenge when using a tethered tug is avoiding post-burn collision between the debris and tug. The residual post-thrust strain in the tether pulls the two bodies toward each other. Reducing strain and the relative motion between the bodies is necessary to remove collision potential. This paper uses two environments for analysis.

- Deep space: the gravitational field is zero, and the six degree-of-freedom rigid body dynamics problem is reduced to a one-dimensional scenario to analyze the challenges of implementing input-shaped thrusting on a multi-mode, tethered-tug debris system
- On-orbit: the LEO environment is used as well as the full six degree-of-freedom dynamics

In the **deep space** analysis, the mass of the debris object is assumed to not be well known. The effect of this uncertainty on the thrust control and post-burn relative velocity is explored. A deep space environment is a reasonable first order assumption for approximating the dynamics of the tethered system during thrusting because the thrust maneuver only lasts a few minutes. The orbital motion and the deep space motion will not vary significantly during thrusting as low Earth orbits have periods around 2 h.

The deep space environment allows for direct analysis of the tethered-tug system's dynamics. However, to operate in LEO **on-orbit** simulations are required. Of interest is investigating how the post-burn relative velocities impact the motion over a few orbits. The tether is also assumed to be taut in this study because a slack tether results in an undesirable whipping behavior, which will not be explored in this paper. Higher order tether modes, whipping motion and end body rotation are all left to future study. Such studies warrant their own investigation because with the rotational motion of the end bodies, the tether stiffness becomes a function of the tether tension. This greatly complicates the use of input shaping techniques. Rather, the presented analysis uses a lumped mass model to set up the input-shaped maneuver, while the simulations use a higher fidelity model which accounts for the full relative translational and rotational motion.

2. Tether model

The tether is modeled as multiple, discrete point masses. Based upon the tether material and volume the overall mass can be found. This is split into one or more, equally spaced mass particles, commonly referred to as a lumped-mass model [17,18]. Each point mass is connected to its nearest neighbors through a spring. This is shown in Fig. 2. This model allows for flexing of the tether as well as the general motion of the tether due to thrusting forces.

For this paper the tug, debris, tether, and simulation parameters are given in Tables 1 and 2. In Table 1 the mass and inertia values for the Tug are similar to the Soyuz upper stage rocket and the debris values are close to the Cosmos-3 M 2nd stage. Kevlar is used as the tether material because it is commonly used in tether analysis [19] and the diameter of 3 mm is chosen to withstand the stresses experienced. In Table 2 a $\sim$2000 N thrust is chosen to be representative for the Soyuz upper stage thrusters while achieving the worst case, maximum tether tension, as described in Ref. [11]. (Note that the 'step-input' thrust linearly ramps on and off, to and from the max thrust over a period of 1 s.) The Δv capability is based upon the fuel reserves that may be available in the Soyuz after delivering a payload to orbit. Finally, the starting altitude of 800 km is based upon the known high density of Cosmos rocket bodies at that altitude and the fact that they are considered high priority targets for ADR [20].

The values in Tables 1 and 2 are used as a case study for this system, motivated by the original Omsk concept of tugging an upper stage rocket body. Ref. [11] discusses that

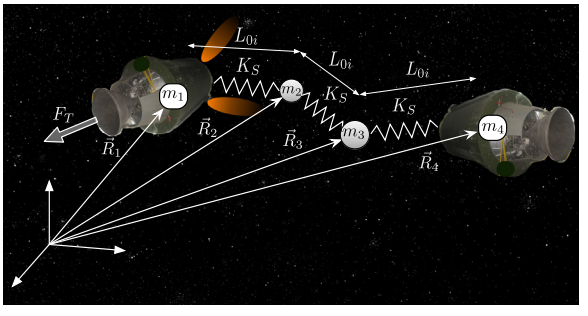

Fig. 2. Tether model: two rigid bodies, two tether point mass.

Table 1
Vehicle parameters.

Tug mass	2500 kg
Tug inertia	diag[10,208, 10,208, 2813] kg m^2
Tug dimensions	$r=1.5$ m, $h=6.5$ m
Debris mass	1500 kg
Debris inertia	diag[1285, 6829, 6812] kg m^2
Debris dimensions	$r=1.2$ m, $h=7$ m
Tether length	1000 m, equal space between masses
Tether material	Kevlar
Young's modulus	1470 GPa
Tether dimensions	$r=1.5$ mm, $h=1000$ km
Tether cross sectional area	7.0686e^{-6} m^2
Tether mass	11.822 kg[a]

[a] http://www.matweb.com/index.aspx.

Table 2
Simulation parameters.

Thrust	2009 N
Δv	100 m/s
Starting altitude	800 km (circular)

the uncontrolled system's behavior could vary noticeably due to tether length and thrust level. Ongoing research is investigating this complex dynamic response to determine what tether length and material properties are preferable when tugging larger upper stage rocket bodies. For the scope of this paper, a single test case is discussed which applies to the original Soyuz-tugging concept. In particular, at this stage damping in the tether material is not considered to illustrate how the coupled gravitational and tension forces alone can cause desirable post-burn motions. Future work will explore the tethered-tug system's design space across different thrust levels, masses and tether properties.

The system is made of two rigid end-masses, $n-2$ discrete tether masses, and a spring-like tether, making an n body equation of motion, shown in Eq. (1).

$$\dot{\boldsymbol{x}} = [A]\boldsymbol{x} + [B] \tag{1}$$

where

$$\boldsymbol{x}_{2n\times 1} = \begin{bmatrix} x_1 \\ \vdots \\ x_n \\ \dot{x}_1 \\ \vdots \\ \dot{x}_n \end{bmatrix}, \quad [B]_{2n\times 1} = \begin{bmatrix} 0 \\ \vdots \\ 0_n \\ \frac{F_T}{m_1} \\ 0_2 \\ \vdots \\ 0_n \end{bmatrix}$$

$$[A]_{2n\times 2n} = \begin{bmatrix} & & [0]_{n\times n} & & & [I]_{n\times n} \\ -\frac{K_S}{m_i} & \frac{K_S}{m_i} & 0 & \cdots & 0_n & \\ \frac{K_S}{m_{i+1}} & -\frac{2K_S}{m_{i+1}} & \frac{K_S}{m_{i+1}} & \ddots & \vdots & \\ 0 & \ddots & \ddots & \ddots & 0_{n-2} & [0]_{n\times n} \\ \vdots & \ddots & \frac{K_S}{m_{n-1}} & -\frac{2K_S}{m_{n-1}} & \frac{K_S}{m_{n-1}} & \\ 0_n & \cdots & 0_{n-2} & \frac{K_S}{m_n} & -\frac{K_S}{m_n} & \end{bmatrix}$$

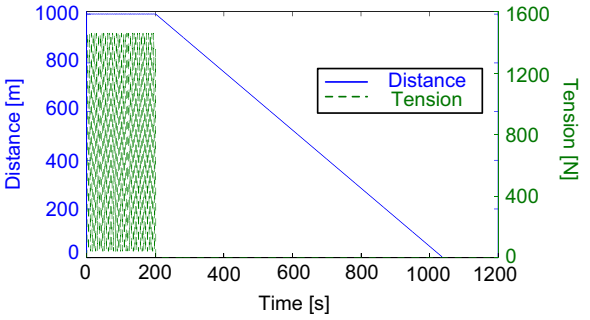

Fig. 3. Relative motion and tether tension response between tug and debris for a step input 2009 N thrust, with two discrete tether masses.

The spring constant K_S can be expressed as shown in Eq. (2).

$$K_S = \frac{EA}{L_{0_i}} \tag{2}$$

Here L_{0_i} is the initial, unstretched length of the tether between each mass, E is the Young's modulus of elasticity for the tether, and A is the cross sectional area. In this study, all L_{0_i} are the same. Because Eq. (1) models a tether as a spring, it is only accurate while the tether is in tension. Eq. (3) demonstrates that the tether spring force for each element is reduced to zero when there is no tension, creating an overall nonlinearity in the system.

$$T_i = \begin{cases} 0 & \text{for } L_i \le L_{0_i} \\ \frac{1}{2} K_S \Delta L_i & \text{for } L_i > L_{0_i} \end{cases} \tag{3}$$

Because the tether only pulls on the masses when in tension, and does not provide a 'pushing' force when in compression, collisions between the large end-masses become possible. This is undesired as collisions could cause more orbital debris, something that is unacceptable from an ADR system. It therefore becomes important to study the complex tether dynamics between high-force and slack tether motion and to control those dynamics. The possibility of collision is illustrated in Fig. 3 that demonstrates the deep space motion simulation results in collisions. The simulation used to produce Fig. 3 uses two discrete tether masses. A general bang–bang thrust profile leaves tension in the tether which pulls the masses together, causing a collision.

When thrusting, the system oscillates between zero tether tension and high tension. This oscillation occurs at the natural frequency(ies) of the system. Therefore, one very effective way to reduce this motion, and collisions, is to remove these natural frequencies.

3. Thruster input-shaping

Input shaping is a common way to remove an undesired frequency response in a linear system [21,22]. For this specific application, a notch filter is used to remove the natural frequency of the tethered system. A brief summary of a notch filter is given for ease of reference.

In the frequency domain, a first order notch filter is defined as

$$g(s) = \frac{s^2+\omega_c^2}{s^2+\mathrm{BW}s+\omega_c^2} \tag{4}$$

where s is the frequency, ω_c is the cut-off or notch frequency, and BW is the bandwidth of the notch filter.

It is also helpful to be able to notch two frequencies at once. This is simply created by multiplying two notch filters together, in the frequency domain, that have different cut-off frequencies.

$$g(s) = \frac{(s^2+\omega_{c1}^2)(s^2+\omega_{c2}^2)}{(s^2+\mathrm{BW}_1 s+\omega_{c1}^2)(s^2+\mathrm{BW}_2 s+\omega_{c2}^2)} \tag{5}$$

ω_{c1} is the first cut-off or notch frequency, ω_{c2} is the second cut-off or notch frequency, and BW_1 and BW_2 are the bandwidths for each notch. Eqs. (4) and (5) can be converted into the discrete domain and the time domain in many ways. This process is not discussed here.

In order to properly reduce motion between the tug and debris, the system's natural frequencies (Eigenvalues) must be known. Because the tether system is modeled as a linear spring when in tension, eigenvalue analysis lends itself perfectly to this model.

Unfortunately, it becomes very difficult to analytically solve for the eigenvalues and frequencies of the tether as more nodes are added. The Abel–Ruffini theorem demonstrates that there are no general algebraic solutions to polynomials of degree five and higher [23,24]. This means that it is not likely that the full set of eigenvalues for tether discretizations beyond three or four nodes is analytically achievable. However, this is not a major concern because the majority of the energy and dynamics of the system come from the first few modes, or eigenvalues. Therefore, the primary modes of interest can be analytically computed for any system. Further, these modes will be the same, independent of the number of discretized nodes placed on the tether.

As an example, the eigen values of two rigid bodies connected by a massless tether are:

$$\omega_n = \begin{pmatrix} 0 \\ 0 \\ -\sqrt{\frac{K_S(m_1+m_2)}{m_1 m_2}} \\ \sqrt{\frac{K_S(m_1+m_2)}{m_1 m_2}} \end{pmatrix} \tag{6}$$

The eigen-frequencies ω_n of a three body (single tether mass) system are

$$\omega_n = \begin{pmatrix} 0 \\ 0 \\ \pm\sqrt{K_S Z_1 + K_S Z_2} \\ \pm\sqrt{K_S Z_3 + K_S Z_4} \end{pmatrix} \tag{7}$$

where

$$Z_1 = \frac{(m_2 m_3 + m_1(m_2+2m_3))}{2m_1 m_2 m_3}$$

$$Z_2 = \frac{\sqrt{m_1^2 m_2^2 - 2m_1 m_2^2 m_3 + (4m_1^2+m_2^2)m_3^2}}{2m_1 m_2 m_3}$$

$$Z_3 = \frac{(-2m_1 m_3 - m_2(m_1+m_3))}{2m_1 m_2 m_3}$$

$$Z_4 = \frac{\sqrt{-2m_1 m_2^2 m_3 + m_2^2 m_3^2 + m_1^2(m_2^2+4m_3^2)}}{2m_1 m_2 m_3}$$

Note that this analytic solution to the eigen frequencies can be used to approximate the first modes of the massive tether independent of the number of discretized masses actually used. Therefore, the first mode of the system with only one tether node is the same as the system with many tether nodes, assuming the masses are unchanged.

The repeated 0 roots relate to the DC offset present in the formulation of Eq. (1). Because Eq. (1) is formulated from the positions of the bodies, the equations naturally assume that zero tether force corresponds to separation distances between the masses that add up to the full tether length (i.e. L_0). Therefore the bodies have a constant, DC offset in their positions. The complex pair(s) in Eq. (7) represent the purely oscillatory motion, as expected from a spring–mass system. Eq. (7) has two sets of complex pairs due to the fact that a three body (single tether node) system has two modes: one from the full tether length and one from the addition of the tether mass.

Again, it is interesting to note that the fundamental frequency is the same between the two-body, three-body, and four-body cases. This turns out to be (for two bodies: $m_1 = 2500$ kg, $m_2 = 1500$ kg; for three bodies: $m_1 = 2500$ kg, $m_2 = 11.82$ kg, and $m_3 = 1500$ kg, for four bodies: $m_1 = 2500$ kg, $m_{2a}+m_{2b} = 5.91+5.91 = 11.82$ kg, and $m_3 = 1500$ kg) $\omega_{n1} = 0.19$ Hz. The three node case also has its second mode at $\omega_{n2} = 3.43$ Hz. Therefore, these can become the notched frequencies used in the input-shaping approach.

4. Deep space numerical results

4.1. Towing in Deep Space

To demonstrate why input shaping (notching) is required, consider Fig. 3 where no shaping method is used during thrusting. Here the thruster cuts off at $\Delta v = 100$ m/s while there still is tension in the tether. The restoring spring force in the tether will pull all masses together and eventually cause a collision, as seen beyond 1000 s in Fig. 3. It therefore becomes imperative to reduce the remaining tether tension to stop post-thrust relative motion between the masses. Jasper et al. [11] demonstrate that the thrust magnitude could (based upon the tether properties and rigid body end masses) be set to achieve the desired Δv without leaving the tether in tension. This method requires well known system properties and the ability to very specifically set the thrust value.

As an alternate control method, the thrust profile could include filtering so that the fundamental frequencies of the tethered system are removed. Using a notch filter (Eq. (4)), the first fundamental mode, shown in Fig. 4(a) at $\omega_n = 0.19$ Hz, is removed and the behavior becomes much more desirable. Figs. 5 and 4(b) show the improvement in the post-thrust dynamics. The relative motion between the tug and the first discrete tether mass is significantly

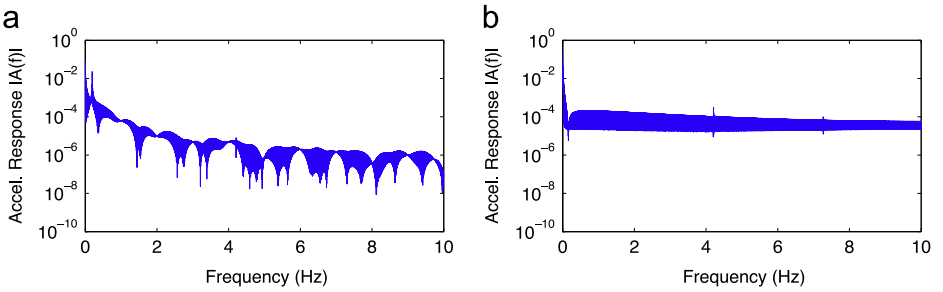

Fig. 4. Tug vehicle frequency response to 2009 N thrust, with two discrete tether masses. Deep space. (a) Step-input thrust profile. (b) Notch at $\omega_c = 0.19$ Hz.

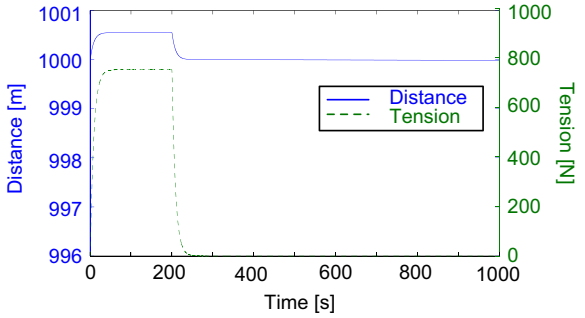

Fig. 5. Relative motion and tether tension response between tug and debris for a single notch with the cut off frequency at the first mode. 2009 N thrust, with two discrete tether masses. Deep space.

reduced, shown in Fig. 5 and there is less than a meter of relative drift between the two. This result is very similar for the relative motion between the other tether masses and the debris. Fig. 4(b) demonstrates the dramatic difference in the response profile. The fundamental mode, seen as the first peak in Fig. 4(a), is heavily attenuated in Fig. 4(b).

Fig. 6 compares the tether mass frequency responses. Note that this response is very similar between both tether masses modeled, therefore only one set of plots is shown. The tether masses are shown here to generally move and oscillate at higher frequencies than the larger rigid bodies. The notching has less of an effect on their behavior however there are subtle reductions in the profile below 1 Hz in Fig. 6(b). Fig. 7 compares the debris behavior between bang-bang and notched thrust profiles. In Fig. 7 (b) it is also obvious that the first mode at 0.19 Hz has been significantly attenuated, as desired.

4.2. Eigen-frequency sensitivity

The notching shown in Fig. 4(b) presents an ideal case where all system parameters are well known. However, if the eigenvalues in Eq. (7) are not well known, the natural frequencies can change from what is expected, lowering the effectiveness of the notch filter. The debris mass (m_3 in Eq. (7)) will be the least well known value in the computations. The linear sensitivity of the natural frequency in Eq. (7) can be found by taking the partial derivative of the natural frequency with respect to m_3 and evaluating at the expected values (given in Table 1, where the expected debris mass $m_{3e} = 1500$ kg). Eq. (8) shows the linear change in the natural frequency given the true debris mass, m_{3t}.

$$\Delta\omega_n(m_{3t}) = \frac{\partial\omega_n}{\partial m_3}\bigg|_{K_S, m_1, m_2, m_{3e}} (m_{3t} - m_{3e}) \tag{8}$$

Evaluating Eq. (8) from $m_{3t} = 600$–2400 kg, Fig. 8 shows that the mass of the debris can vary by 900 kg (60%) and it will only change the first mode by 0.03 Hz. Because the first mode contains the most energy for the system this mode will be focused on. Given the tether properties, masses of the tug and debris, the first mode should occur near 0.19 Hz. It turns out that a variance of 0.03 Hz in the first mode is enough to cause the notch filter to have significant, but relatively small, performance problems. One robust method to avoid sensitivity issues is to add a second notch in the region of the first mode.

To design a double notch around the first mode, Fig. 8 is used to determine the potential range over which the first mode can vary. When two notches are placed near each other, they effectively attenuate a range of frequencies. This behavior can be seen in Fig. 9 where frequencies 0.14–0.22 Hz are very heavily notched. While there is reduced attenuation between these two frequencies it is still very large, peaking near -58 dB (half way between the notched range, at 0.18 Hz). This is sufficient to reduce the first mode's energy.

Using this type of double notch while including errors in debris mass knowledge, significant reductions in relative motion are still produced (Fig. 10). Fig. 10(a) shows that the single notch placed at the expected, but incorrect, natural frequency experiences small but noticeable collapse of the system. Conversely, Fig. 10(b) shows that the double notch effectively reduces the motion between the masses, even though the exact natural frequency is not well known. It turns out that the relative motion of the masses is reduced nearly as well as the perfect single notch of Fig. 5. The performance difference between the single notch and the double notch spanning a wide range of frequencies can be seen in Fig. 11. The double notch experiences more attenuation of the first mode, compared to the improperly placed single notch. The double notch frequency response does see less attenuation near 0.2 Hz,

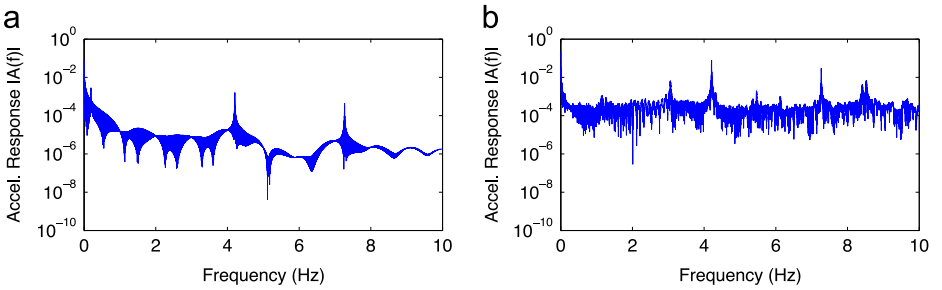

Fig. 6. Tether mass frequency response to 2009 N thrust, with two discrete tether masses. Deep space. (a) Step-input thrust profile. (b) Notch at $\omega_c = 0.19$ Hz.

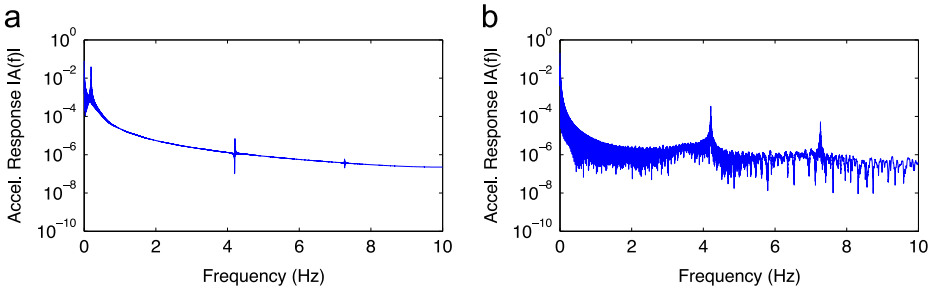

Fig. 7. Debris object frequency response to 2009 N thrust, with two discrete tether masses. Deep space. (a) Step-input thrust profile. (b) Notch at $\omega_c = 0.19$ Hz.

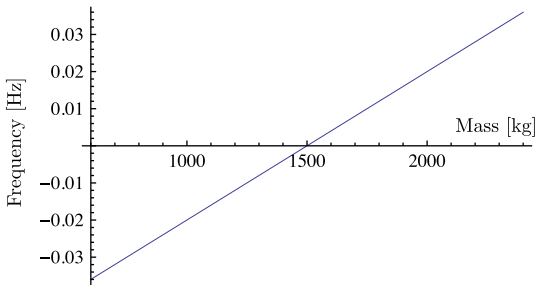

Fig. 8. Sensitivity of the tether-mass system's first fundamental mode ($\omega_n = 0.19$ Hz) to imperfect debris mass knowledge.

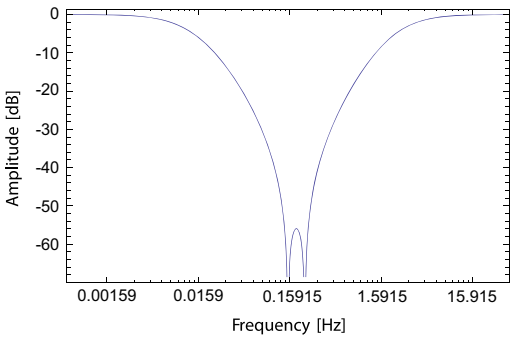

Fig. 9. Double notch centered about first fundamental mode of system.

in the same location as the 'hump' in Fig. 9, which is expected.

While the debris mass will be the least well known, the tether spring constant may have variability as well. Because the natural frequencies are very dependent upon this parameter, it is important to consider. Using a similar linear sensitivity analysis to in Eq. (8), the system's natural frequency response to variable material properties is

$$\Delta\omega_n(K_{St}) = \left.\frac{\partial\omega_n}{\partial K_S}\right|_{K_{Se},m_1,m_2,m_3} (K_{St} - K_{Se}) \tag{9}$$

Evaluating Eq. (9) across a 20% change from the expected spring constant ($K_{Se} \approx 4100$ N/m, between each node), Fig. 12 is obtained. Note that a 20% change in spring constant is approximately equal to a Young's modulus change of 34 GPa or a 0.7 mm change in the radius of the tether, both fairly large numbers. However, these can be considered worst case and they achieve similar variability in the natural frequency to a 500 kg change in debris mass. When the input shaping capabilities are compared between the single and double notch for spring constant variability (Fig. 13), it can again be seen that the double notch successfully reduces the relative motion between the two end bodies (Fig. 13(b)) when compared to the single notch (Fig. 13(a)).

Notching does cause phase lag in the thrust profiles and the system responses. Therefore the thrust period of a step input is shorter than a single or double notch. This behavior is shown in Fig. 14. It takes the step input (no shaping) about 201 s to achieve a $\Delta v = 100$ m/s while the single notch takes 238 s and the double notch 283 s to reach within about 1% of a 0 N thrust. This means that it takes less than 5 min for any of these methods to perform their burn, a time duration which is very short when considering an orbital period of around 90 min in LEO.

This demonstrates that the double notch spanning the possible range of the first mode can effectively reduce collision potential between the masses with large uncertainties in the debris mass and tether material properties. This also demonstrates that the first mode is the most

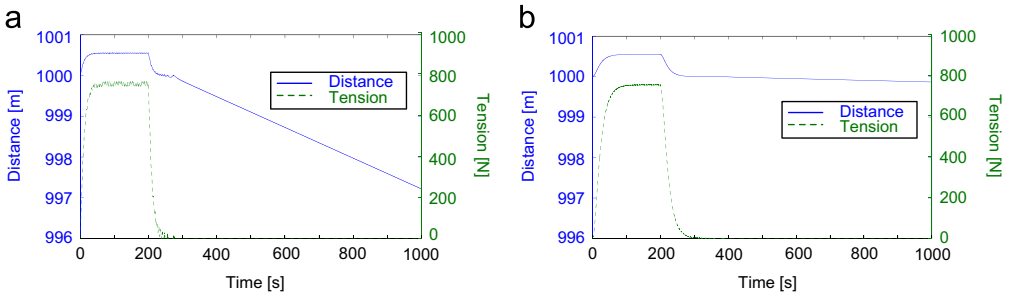

Fig. 10. Relative motion and tether tension response between tug and debris for an expected debris mass of 2000 kg ($\omega_n = 0.17$ Hz), actual mass is 1500 kg ($\omega_n = 0.19$ Hz). 2009 N thrust, with two discrete tether masses. (a) Single notch, $\omega_c = 0.17$ Hz. (b) Double notch spanning $0.14 \le \omega_c \le 0.22$ Hz.

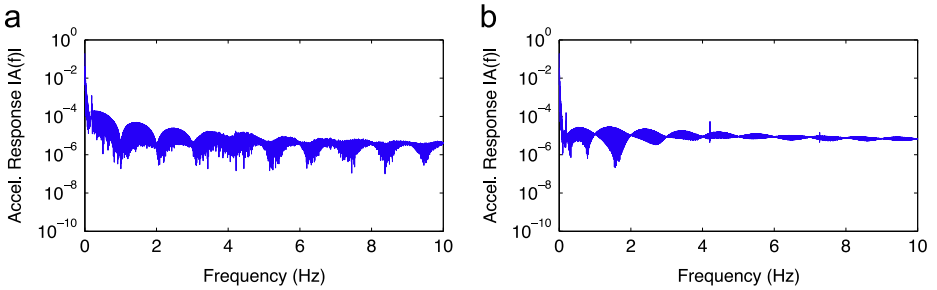

Fig. 11. Tug vehicle frequency response with two discrete tether masses. Expected $\omega_n = 0.17$ Hz, actual $\omega_n = 0.19$ Hz. (a) Single notch, $\omega_c = 0.17$ Hz. (b) Double notch spanning $0.14 \le \omega_c \le 0.22$ Hz.

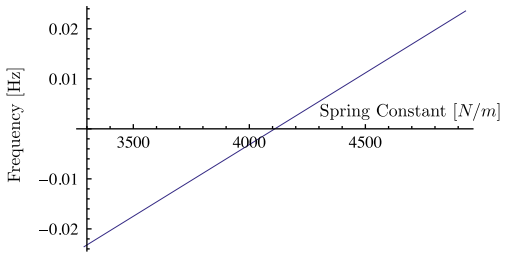

Fig. 12. Sensitivity of the tether-mass system's first fundamental mode ($\omega_n = 0.21$ Hz) to variable spring constant.

important because nearly all relative motion is stopped by notching only the first mode, while leaving the other modes unshaped. Tether models can become very complex (using partial differential equations and finite element solvers). It is significant to determine that the first mode is the only mode that needs to be notched because it is the most simple mode to model and analyze. This may help to drastically reduce the analysis required for a tether–tug system.

5. Effects of a slack tether in deep space

Having a slack tether can drastically change performance of the system. All previous simulations presented in this paper have assumed that both objects are initially separated by the tether length of 1000 m. That is, the tether is virtually taut when the thrust starts. Conversely, Fig. 15 shows how a slack tether amplifies the dynamic response of the system while removing all effects of input shaping. A collision occurs near 400 s and the tether force jumps to near 27,000 N, not 800 N seen in Fig. 10(b).

This is caused by the fact that the majority of the input shaped thrust profile occurs during the time it takes to remove the slack in the tether and pull it taut. The tether does not see a gradual increase in force but a large step increase all while the tug is increasing in velocity. This causes the large 'whipping' effect seen in Fig. 15.

It is important to reduce the slack length in the tether. Ways to counter this effect are left for future work but several methods could be employed. One method would be to allow the two end bodies to drift apart in orbit. Once a small tension force in the tether started to build the thruster could be activated. The overall effectiveness of any tether tightening method needs to be analyzed for it ability to avoid high tether stress and collisions.

The following section, concerning input shaping on-orbit, assumes that the tether starts taut.

6. On-orbit numerical results

6.1. Thrust input shaping on-orbit

To show the effectiveness of this method when on-orbit, a four mass (two tether mass) system is used with a double notch spanning across the first mode as shown in Fig. 9. While the system's actual natural frequency is 0.19 Hz, the double notch allows for uncertainties in debris mass knowledge. The debris and tug craft are started in an 800 km circular orbit and a burn is produced in the anti-velocity direction to lower both object's orbits. A $\Delta v = 100$ m/s lowers the periapsis to about 425 km.

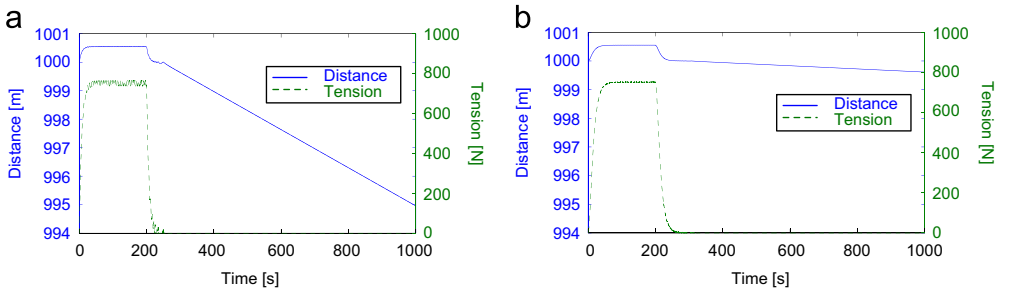

Fig. 13. Tug vehicle frequency response to spring constant variability with two discrete tether masses. Expected $\omega_n = 0.17$ Hz, actual $\omega_n = 0.21$ Hz. (a) Single notch, $\omega_c = 0.17$ Hz. (b) Double notch spanning $0.15 \leq \omega_c \leq 0.25$ Hz.

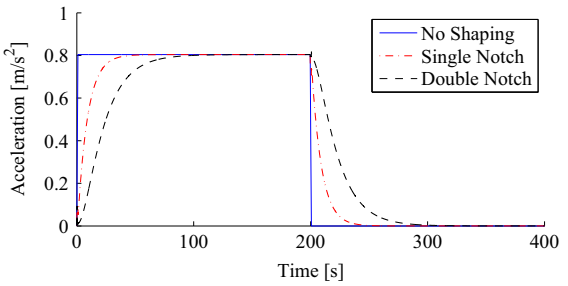

Fig. 14. Thrust profiles with different input shaping techniques.

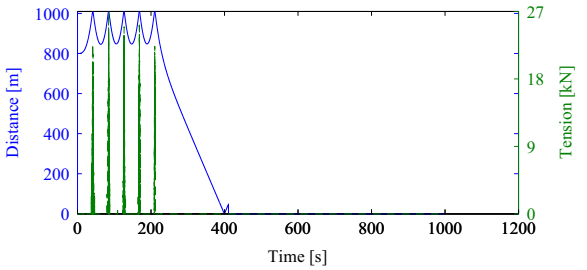

Fig. 15. Slack tether: 1000 m tether with 200 m of slack. Simulated in deep space with a double notch ($0.14 \leq \omega_c \leq 0.22$ Hz), assuming a debris mass of 2000 kg (actual 1500 kg), 2009 N thrust, two discrete tether masses. Deep space.

The double notch in Fig. 16(b) experiences separation distances that are just as small as the step-input thrust of Fig. 16(a) which is unexpected from the deep space simulations. However, there are several new advantages to input shaping that are not apparent in the deep space simulations. The step input system tumbles but the notched system quickly settles into a gravity gradient type configuration where the masses have aligned along the radial vector, and after one orbit, remain about the full tether length apart from each other. The notched system's oscillation about the radial vector (a nadir alignment) is shown in Fig. 17 where the notched motion oscillates about 90° from the in-track direction. Conversely, the step input only experiences tumbling with a large range of separation distances between the bodies. The fact that the notched system achieves a gravity gradient orientation is very encouraging and would help to keep these masses separated for their orbital lifetime. It is also encouraging to note that the tether tension forces are noticeably reduced in Fig. 16(b) placing less stress on the entire system.

6.2. Orbital decay rates

The effectiveness of lowering the system's perigee is shown in Table 3. On-orbit lifetime is modeled using drag coefficients for cylinders [25] that range between 2.4 and 2.9 assuming the long axis of the cylinders is directly into the ram-vector. The atmospheric temperatures are assumed not to vary significantly. The computation of drag coefficients of general shapes is complex and is still an active area of research. For the purpose of this study, simplified drag coefficients suffice as only approximate decay lifetimes are being determined. The tug and debris are assumed to be cylindrical bodies and the drag force is computed for each object and then summed about the center of mass. The tether is not included in this analysis due to the difficulty of determining the drag coefficient of such a large and thin structure. This means that the lifetimes obtained should actually be less than those given in Table 3. The ballistic coefficients under consideration fall between 0.0459 and 0.0555.

If no ADR or mitigation system is used, a circular orbit of about 700 km takes two to three decades to deorbit, a 800 km takes 50–70 years to deorbit while a 1000 km orbit takes more than a century [1]. By reducing the periapses to the 300–400 km range, the tethered-tug system significantly reduces these time scales to less than 5 years, a major improvement. The elliptical 800 km by 425 km post-burn orbit used in this paper (Table 3, in bold) deorbits in about 3–5 years, much shorter than the natural decay rate or the 25 year requirement. If more residual fuel is present, a direct reentry maneuver is also feasible. However, as this table illustrates, using the small Δv to lower the periapsis of the tethered system has a significant impact on the debris' decay time.

7. Conclusions

A second stage rocket body with fuel reserves could be used as an ADR system. With a tether as an energy transfer mechanism and a thrust applied by the rocket, the periapses of both objects can be significantly lowered. This allows for drag to affect their orbits more, reducing lifetimes. Step input (impulsive) thrust profiles were shown to be challenging for a tethered ADR system due

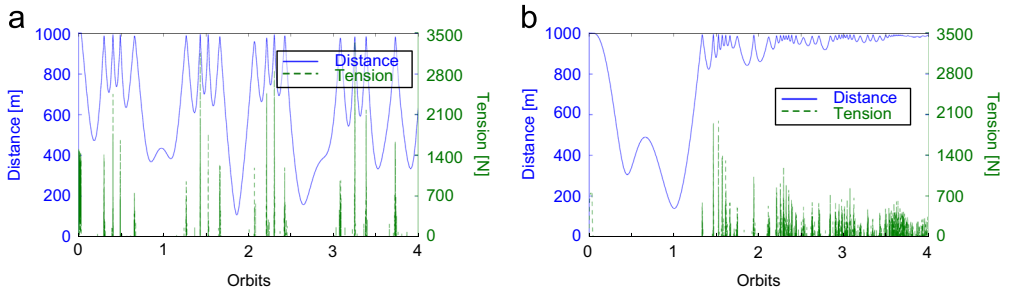

Fig. 16. Relative motion and tether tension response between tug and debris for four orbits. Tether $\omega_n = 0.19$ Hz. 2009 N thrust, with two discrete tether masses. (a) Step-input thrust profile. (b) Double notch spanning $0.14 \le \omega_c \le 0.22$ Hz.

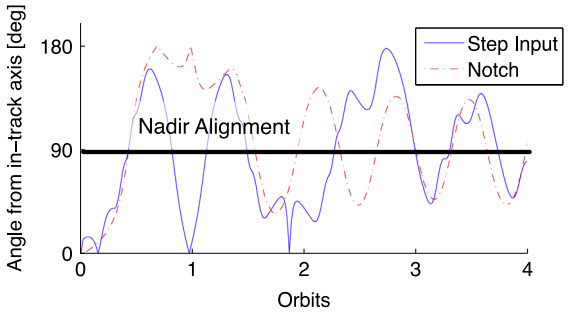

Fig. 17. Angle from along-track vector. 90° is the radial vector.

Table 3
Lifetime of tethered-tug system using Jacchia 1977 atmosphere model [26].

Perigee	Apogee	Drag coefficient	Circ. orbit at apogee (years)	Post-maneuver (years)
350	700	2.4	27.72	0.74
		2.9	25.22	0.57
425	700	2.4	27.72	1.93
		2.9	25.22	1.56
350	800	2.4	73.39	0.99
		2.9	53.84	0.82
425	**800**	**2.4**	**73.39**	**2.71**
		2.9	**53.84**	**2.22**
350	1000	2.4	> 100	1.48
		2.9	> 100	1.19
425	1000	2.4	> 100	4.39
		2.9	> 100	3.66

to the chaotic motion, collision potential, and high tether tensions induced. It was shown that the majority of the relative motion that occurred between both craft is due to the tether's first fundamental mode. Reducing energy input into the system at this frequency, through thrust input shaping, effectively reduced these problems. It was also shown that the first mode of the tethered system is the most important to reduce frequency input. This is very encouraging because this mode is only affected by the tether material properties and length, not the number of discretized masses or any other variable property. This means that the tether motion can be effectively modeled and studied without incredibly high-fidelity tools.

Input shaping while on-orbit results in the masses achieving a gravity gradient-like formation which will allow for separation distances to be maintained between bodies. This is very encouraging and future work may consider a tether with damping and longer lengths of tether to achieve more stable gravity gradient orientations. It is therefore likely that this type of ADR system would be practical to design and implement on-orbit.

Acknowledgments

The authors would like to acknowledge Valery Trushkyakov, Professor in the Department of Aviation and Rocket Building, Omsk State Technical University for his contributions to the tethered rocket body ADR method.

References

[1] E. Stansbery, NASA Orbital Debris Program Office Frequently Asked Questions, NASA, Lyndon B. Johnson Space Center Houston, Texas, 2012.
[2] C. Pardini, L. Anselmo, Evolution of the debris cloud generated by the fengyun-1c fragmentation event, in: 20th International Symposium on Space Flight Dynamics, Goddard Space Flight Center Greenbelt, MD, 2007, NASA CP-2007-214158.
[3] T. Kelso, CelesTrak, CSSI Center for Space Standards and Innovation, ⟨http://celestrak.com/⟩, 2012.
[4] N.L. Johnson, Orbital debris: the growing threat to space operations, in: 33rd Annual AAS Guidance and Control Conference, Breckenridge, CO, 2010.
[5] C. Pardini, L. Anselmo, Physical properties and long-term evolution of the debris clouds produced by two catastrophic collisions in earth orbit, Adv. Space Res. (2011) 557–569.
[6] D.J. Kessler, B.G. Cour-Palais, Collision frequency of artificial satellites: the creation of a debris belt, Geophys. Res. 83 (1978) 2637–2646.
[7] J.-C. Liou, N.L. Johnson, Risks in space for orbiting debris, Science 311 (2006) 340–341.
[8] J.-C. Liou, N. Johnson, N. Hill, Controlling the growth of future leo debris populations with active debris removal, Acta Astronaut. 66 (2010) 648–653.
[9] D. Alary, Astrium's views on oos & adr, in: European On-Orbit Satellite Servicing and Active Debris Removal Conference, Brussels, Belgium, 2012.
[10] C. Bonnal, C.R. Koppel, Getting rid of large debris: a safe low cost alternative, in: 2nd European Workshop on Active Debris Removal, Quentin, Paris, France, Paper No. 3.2, 2012.
[11] L. Jasper, H. Schaub, C. Seubert, T. Valery, E. Yutkin, Tethered tug for large low earth orbit debris removal, in: AAS/AIAA Astrodynamics Specialists Conference, Charleston, SC, Paper No. AAS 12-252, 2012.
[12] J. Reed, J. Busquets, C. White, Grappling system for capturing heavy space debris, in: 2nd European Workshop on Active Debris Removal, Quentin, Paris, France, Paper No. 4.2, 2012.

[13] I. Retat, B. Bischof, J. Starke, W. Froth, K. Bennell, Net capture system, in: 2nd European Workshop on Active Debris Removal, Quentin, Paris, France, Paper No. 4.3, 2012.
[14] V. Trushlyakov, J. Makarov, G. Raykunov, J. Shatrov, D. Baranovo, The development of autonomous onboard systems for the controlled deorbiting of stages separating parts of space launch vehicle, in: 2nd European Workshop on Active Debris Removal, Quentin, Paris, France, Paper No. 2.5, 2012.
[15] M.P. Cartmell, D.J. McKenzie, A review of space tether research, Progr. Aerosp. Sci. 44 (2008) 1–21.
[16] M. Cosmo, E. Lorenzini, Tetheres in Space Handbook, 3rd ed. Smithsonian Astrophysical Observatory. Prepared for NASA Marshall Space Flight Center, Cambridge, MA, 1997.
[17] M. Kim, C.D. Hall, Control of a rotating variable-length tethered system, Adv. Astronaut. Sci. 114 (2003) 1713–1732.
[18] P. Williams, Dynamic multibody modeling for tethered space elevators, Acta Astronaut. 65 (2009) 399–422.
[19] J.A. Carroll, J.C. Oldson, Tethers for small satellite applications, in: AIAA/USU Small Satellite Conference, Logan, Utah, 1995.
[20] J.-C. Liou, An active debris removal parametric study for leo environment remediation, Adv. Space Res. 47 (2011) 1865–1876.
[21] W.E. Singhose, A.K. Banerjee, W.P. Seering, Slewing flexible spacecraft with deflection-limiting input shaping, J. Guid. Control Dyn. 20 (1997) 291–298.
[22] D. Lewis, G.G. Parker, B. Driessen, R.D. Robinett, Comparison of command shaping controllers for suppressing payload sway in a rotary boom crane, in: International Conference on Control Applications, Kohala Coast, Hawaii, 1999, pp. 719–724.
[23] O. Ore, Niels Henrik Abel: Mathematician Extraordinary, 1st ed. University of Minnesota Press, 1957.
[24] R.G. Ayoub, Paolo Ruffini's contributions to the quintic, Arch. Hist. Exact Sci. 23 (1980) 253–277.
[25] M.D. Pilinski, B.M. Argrow, S.E. Palo, B.R. Bowman, Semi-empirical satellite accommodation model for spherical and randomly tumbling objects, J. Spacecr. Rockets 50 (2013) 556–571.
[26] J.D. LaFontaine, P. Hughes, An analytic version of Jacchia's 1977 model atmosphere, Celestial Mech. (1983) 3–26.